

Glycerol dehydrogenation steps on Au/C surface in alkaline medium: An in-situ ATR-FTIR approach



E.H. Fontes^a, C.E.D. Ramos^a, C.A. Ottoni^b, R.F.B. de Souza^a, E. Antolini^c, A.O. Neto^{a,*}

^a Instituto de Pesquisas Energéticas e Nucleares, IPEN/CNEN-SP, Av. Prof. Lineu Prestes, 2242 Cidade Universitária, CEP 05508-900, São Paulo, SP, Brazil

^b Biosciences Institute, São Paulo State University - UNESP, Coastal Campus, Cep: 11330-900, São Vicente, Brazil

^c Scuola di Scienza dei Materiali, Via 25 aprile 22, 16016, Cogoletto, Genova, Italy

ARTICLE INFO

Article history:

Received 10 September 2020

Received in revised form

16 November 2020

Accepted 7 December 2020

Available online 9 December 2020

Keywords:

Glyceraldehyde

Integral equation formalism for polarizable continuum model

Glycerol oxidation reaction

ABSTRACT

The glycerol oxidation reaction (GLYOR) was evaluated using an Au/C electrocatalyst under alkaline conditions and varying glycerol (GLY) concentration. This electrocatalyst was synthesized by the borohydride reduction method. Au/C was characterized by X-ray diffraction (XRD), transmission electron microscopy (TEM), and electrochemical techniques associated with *in situ* attenuated total reflectance Fourier transformed infrared spectroscopy (ATR-FTIR). XRD diffractograms showed the presence of Au (fcc). Cyclic voltammetry assisted by ATR-FTIR *in situ* measurements revealed that GLY oxidation on gold leads to the formation of a high amount of glyceraldehyde (GLYAD) for low GLY concentrations, while a lower amount of GLYAD was observed and the formation of dihydroxyacetone (DHA) was prevalent for high GLY concentrations. For high GLY concentrations DHA is almost stable, whereas for low GLY concentration DHA is fast oxidized to hydroxypyruvate. The excellent GLYOR activity of the Au/C catalyst in low GLY concentrations leads to the formation of deeper oxidized C1 species.

© 2020 Elsevier Ltd. All rights reserved.

1. Introduction

Recently, glycerol (GLY) has been oversupplied due to biodiesel increase production, so this has attracted attention for its use in industrial and energy applications [1]. Likewise, the heterogeneous catalysis community has been focused on developing materials that can transform GLY into valuable compounds, such as glyceraldehyde (GLYAD), dihydroxyacetone (DHA), glyceric acid, and glycolic acid [1–7].

GLYAD has many practical applications on medicine and the organic chemistry field [1], while DHA has been widely used for cosmetics due to its sunless tanning effect [8]. Both of them correspond to the initial stages of the glycerol oxidation reaction (GLYOR), e.g., the GLY dehydrogenation steps. Moreover, an efficient process of GLY dehydrogenation facilitates C–C bond cleavage [9].

It was observed that the initial stages of GLYOR on Pt and Pd were improved in alkaline medium. Zhang and co-workers [7] reported that Au materials have high selectivity to glyceric acid; thereby, GLYAD was also indirectly verified. Furthermore,

supported Au nanoparticles, Au/C, have a high tolerance against oxidation, a good tolerance against metal leaching, a high selectivity to products of a given reaction, and a suitability for aerobic oxidation of CO, H₂, C_nH_m, and alcohols [10].

Zope et al. [10] has reported the beneficial effects of using molecular oxygen species in liquid water to provide a sustainable and environmentally benign alternative to the traditional process that uses expensive inorganic oxidants and harmful organics solvents. Furthermore, the environment in which the electrochemical and spectroelectrochemical experiments are carried out contains a significant amount of liquid water, which turns out to play a significant role in the catalysis. A remarkable feature reported in the literature [10–12] is that molecular oxygen participates in the catalytic cycle not by dissociation to atomic oxygen but by regenerating hydroxide ions formed via the catalytic decomposition of a peroxide intermediate.

Liu and Greeley [9] also reports that there is a third intermediate that is possible to be measured experimentally, and it is a product of the GLY 2H dehydrogenation, namely, 1,2,3-propentriol. With this in mind and considering the reaction mechanism reported by Coutanceau [13], a GLYOR mechanism in alkaline medium is shown in Fig. 1.

The aim of this work is to investigate the products of GLYOR by

* Corresponding author.

E-mail address: aolivei@ipen.br (A.O. Neto).

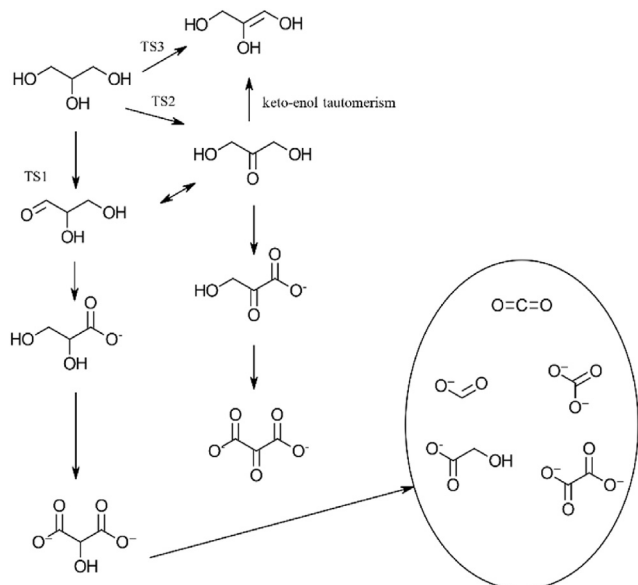


Fig. 1. GLYOR mechanism in alkaline medium. The TS_{1, 2, 3} represents the Transition States.

an *in situ* ATR-FTIR experiment and by cyclic voltammetry. Besides that, we also aim to study the effect of GLY concentration on the type of GLY oxidation intermediate species for a fixed KOH concentration.

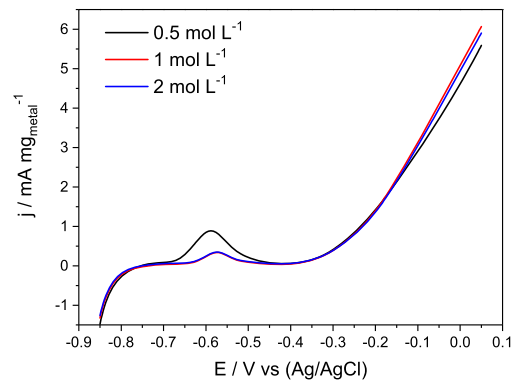


Fig. 3. Linear sweep voltammograms for GOR on Au/C electrocatalyst in KOH 1.0 mol L⁻¹ and glycerol 0.5, 1.0, and 2.0 mol L⁻¹, $v = 10 \text{ mV s}^{-1}$.

2. Methods

2.1. Experimental

Au/C electrocatalysts (20% w/w) were prepared by the sodium borohydride method [14–16], in which H₂HAuCl₄·3H₂O (Aldrich) is the metal source. The metal salt H₂HAuCl₄·3H₂O was added to a mixture of water/2-propanol (50/50, v/v), and then Vulcan XC72 was added. The new resulting mixture was submitted to an ultrasonic bath for 10 min, where a solution of sodium borohydride (Aldrich) was added under stirring at room temperature. After the metal salt reduction, the mixture was filtered, and the solid was washed with water and dried at 70 °C for 2 h.

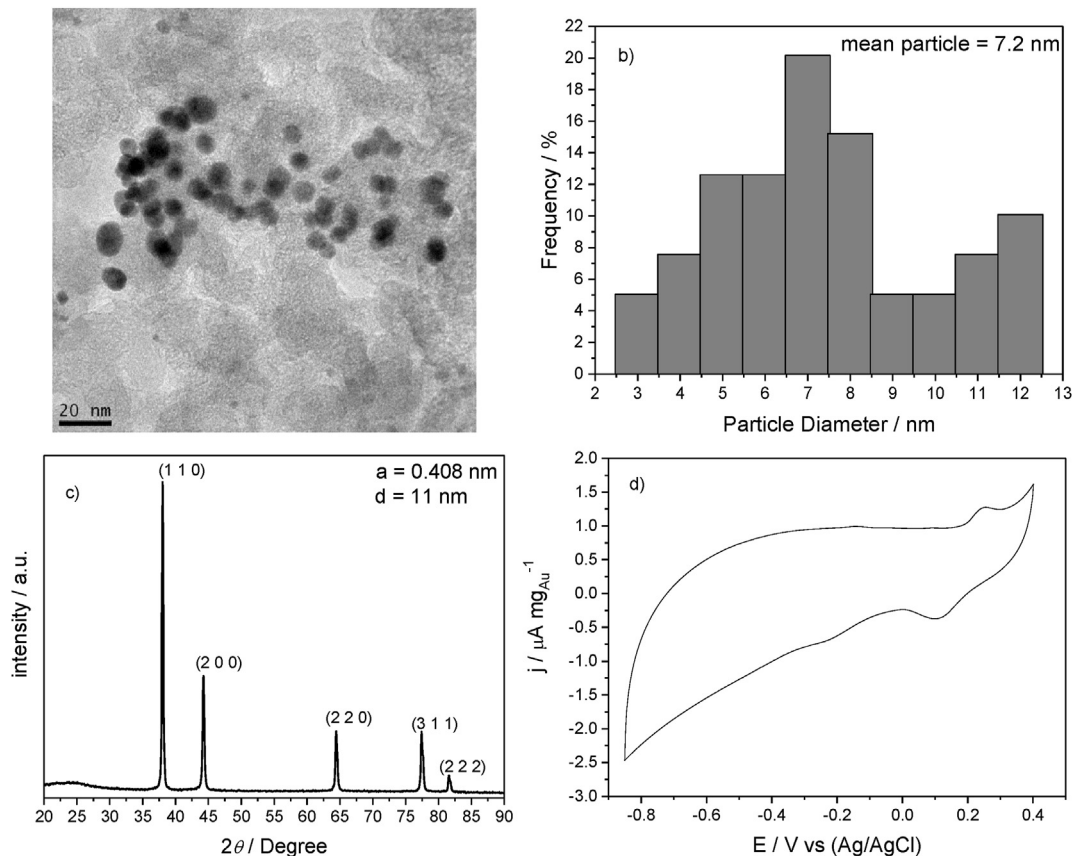


Fig. 2. a) TEM image, b) size distribution histogram, c) XRD patterns, and d) cyclic voltammogram of Au/C catalysts in KOH 1.0 mol L⁻¹ aqueous solution ($v = 20 \text{ mV s}^{-1}$) at room temperature.

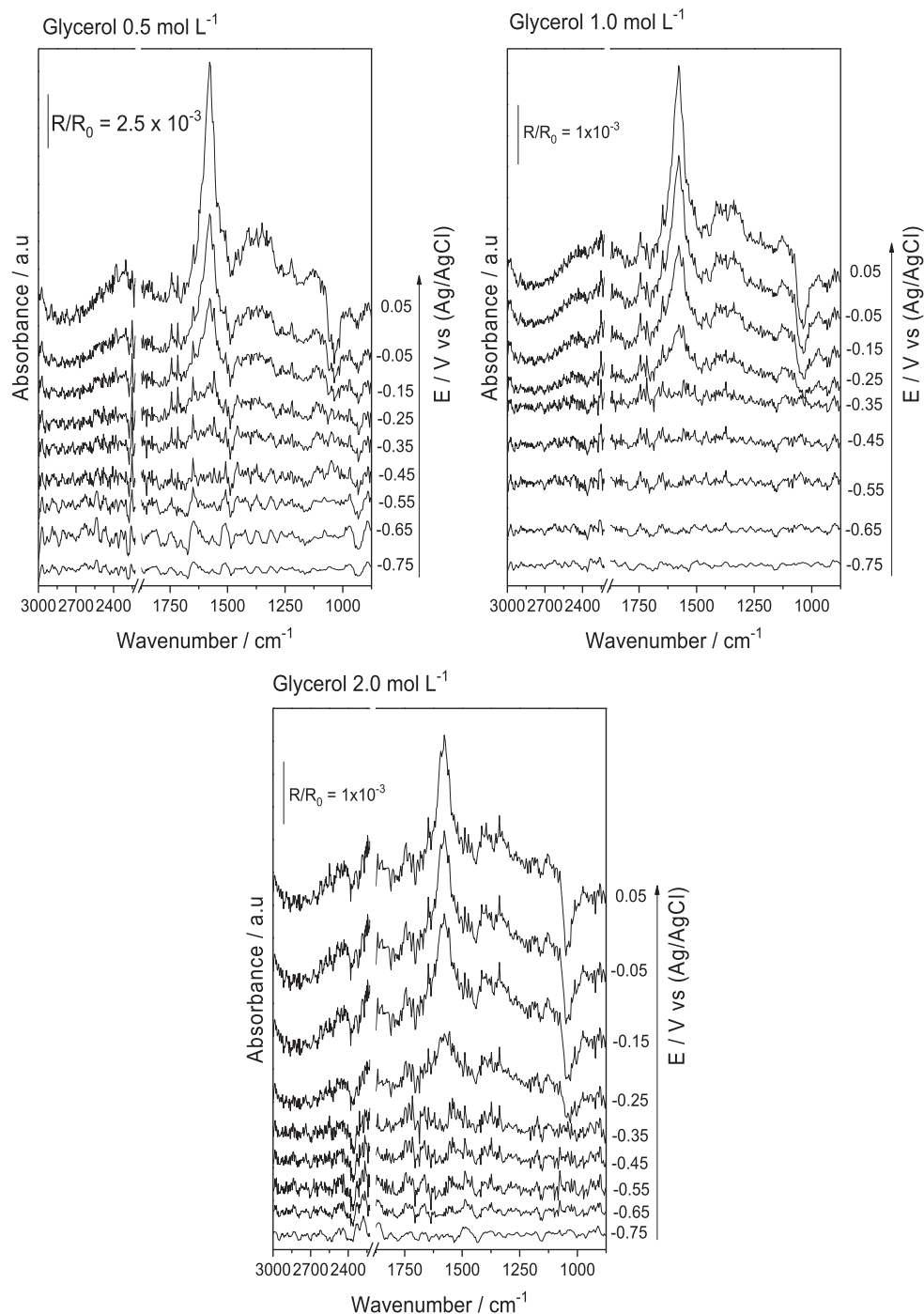


Fig. 4. *In-Situ* ATR-FTIR spectra for GLYOR in different concentrations (KOH 1.0 mol L⁻¹ + glycerol) on Au/C taken at -0.75 to 0.05 V. Backgrounds collected at -0.85 V.

Transmission Electron Microscopy (TEM) was carried out using a Jeol JEM-100 CXII electron microscope at a potential voltage of 80 kV. The TEM images provided us to measure the nanoparticle distribution by counting 150 distinct ones in size and shape. X-Ray Diffraction (XRD) measurements were realized in a Miniflex II model Rigaku diffractometer (CuK α λ = 1.54056 Å) in the range of 20–90° with a step size of 0.05° and scan time of 2 s per step.

The electrochemical experiments were carried out using a three-electrode cell. The working electrode was prepared according to Ref. [16,17], and this coating technique requires 20 mg of powder electrocatalyst placed in a solution of 50 mL of water and 100 μ L of 6% polytetrafluoroethylene (PTFE). The resulting mixture was

treated in an ultrasound bath for 10 min, filtered, and deposited on the working electrode (0.36 cm² area and 0.30 mm deep). The reference electrode was an Ag/AgCl (3.0 mol L⁻¹ KCl), and the counter electrode was a Pt plate. Electrochemical measurements were made using a Potentiostat–Galvanostat Autolab 302 N. Cyclic voltammetry was performed using 0.5, 1.0, and 2.0 mol L⁻¹ glycerol in 1.0 mol L⁻¹ KOH solution saturated with N₂.

The spectro-electrochemical *in situ* ATR-FTIR measurements were performed with Nicolet 6700 FT-IR spectrometer equipped with an MCT detector cooled with liquid N₂, ATR accessory (MIRacle with a Diamond/ZnSe Crystal Plate Pike®), and an electrochemical cell better explained in the literature [16,18,19]. The

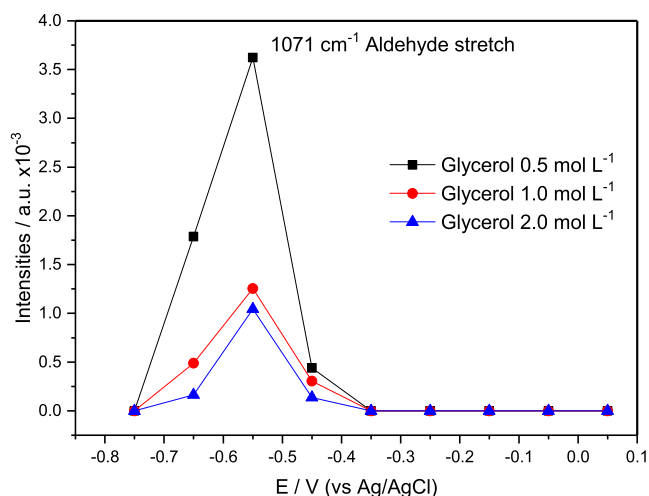


Fig. 5. Glyceraldehyde (aldehyde stretch) integrated intensities bands as a function of the applied bias voltage. Data extracted from Fig. 4.

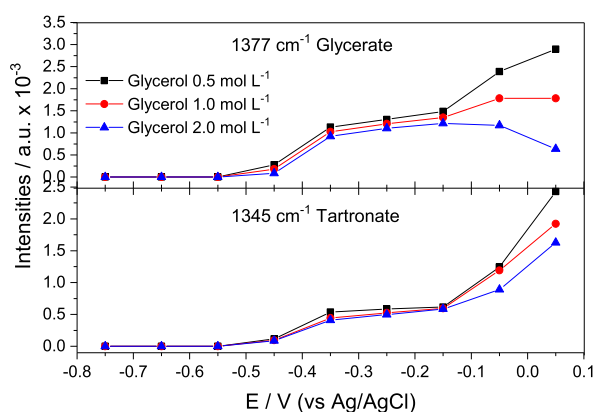


Fig. 6. Glycerate and Tartronate integrated intensities bands as a function of the applied bias voltage. Data extracted from Fig. 4.

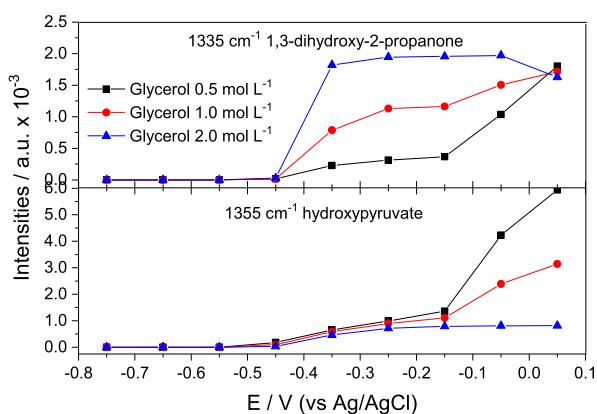


Fig. 7. DHA and hydroxypyruvate integrated intensities bands as a function of the potential. Data extracted from Fig. 4.

working electrodes are the same as the electrochemical experiments in the presence of 0.5, 1.0, and 2.0 mol L⁻¹ glycerol + 1 mol L⁻¹ KOH. The absorbance spectra were collected, such as to obey the ratio R/R_0 , where R represents a spectrum at a given potential, and R_0 is the spectrum collected at -0.85 V. Positive and

negative directional going bands represent gain and loss of species at the sampling potential, respectively. To adequately address the effects of the species production, all bands were deconvoluted to Lorentzian line forms [18]. The spectra were computed from the average of 96 interferograms from 3000 cm⁻¹–850 cm⁻¹ with the spectral resolution set to 8 cm⁻¹.

3. Results and discussion

Fig. 2 shows the physical-chemistry characterization of the Au/C electrocatalyst [7]. Regarding the TEM images (Fig. 2a), it was observed that the Au nanoparticles are well dispersed, although some aggregations can be seen on the carbon powder. The nanoparticles size distribution (Fig. 2b) was (7.2 ± 5.2) nm, which is similar to the results observed in the literature [19,20].

The XRD patterns (Fig. 2c), collected in the range from 20° to 90°, displays a face-centered cubic (FCC) pattern for Au [15], with diffraction peaks at $\sim 39^\circ$, $\sim 46^\circ$, $\sim 66^\circ$, and $\sim 80^\circ$ assigned to the corresponding crystalline planes (111), (200), (220), and (311), peaks, respectively. The Bragg peak in 25° is assigned to the graphitic (002) face of the carbon support [21,22]. The Au lattice parameter was 0.408 nm, which is similar to JCPDS # 04-0784.

The cyclic voltammogram of Au/C catalysts in KOH 1.0 mol L⁻¹ is shown in Fig. 2d: in the region of -0.85 V to -0.1 V a profile similar to Vulcan carbon is observed [23]; furthermore, at 0.25 V in the forward scan a 0.1 V in the reverse scan the peaks related to the defined redox process associated with $Au^0 \leftrightarrow Au^{3+} + 3e^-$ are visible [19,24].

Fig. 3 shows the linear sweep voltammogram profiles obtained during the GLYOR on Au/C in different GLY concentrations. It was observed that for all concentrations, a similar onset potential for GLYOR was found (-0.36 V). All the profiles also showed a peak between -0.6 V and -0.55 V. This peak is due to the formation of GLYOR, as reported by Ottoni [19]. It is important to stress out that for GLYOR (in all concentrations), the profile for GLYOR is very similar in the range of -0.4 V to -0.1 V, indicating that the kinetic limit of turnover was reached.

The *in situ* ATR-FTIR spectroscopy (Fig. 4) was employed to understand the reaction pathways under experimental conditions. Fig. 4 shows a strong band of about ~ 1589 cm⁻¹ corresponding to an H–O–H deformation of water [25]. From -0.15 V up to 0.05 V is possible to identify negative bands related to GLY consumption bands (1004, 1041 and 1094 cm⁻¹) [25,26]. It was also observed an increase of bands that can be attributed to GLYAD at 1071 cm⁻¹ [27], formate at 1225 cm⁻¹ [28], 1,3-dihydroxy-2-propanone/DHA at 1335 cm⁻¹ [29], tartronate at 1345 cm⁻¹ [30], hydroxypyruvate at 1355 cm⁻¹ [25,26], glycerate at 1377 cm⁻¹ [3,29,31], carbonate at ~ 1405 cm⁻¹ [25], carbonyl and carboxyl stretches at ~ 1665 cm⁻¹ [3,25] and carboxyl stretching at 1723 cm⁻¹ [2,25]. CO₂ (2343 cm⁻¹) and Mesoxalate [13,32] signals was not detected in these experiments.

Some studies [9,31,33,34] have proposed that the GLYOR takes place by two main routes (Fig. 1). The first route can start with the dehydrogenation of the primary hydroxy group leading the formation of GLYAD species. At the same time, the other path can occur by dehydrogenation of the secondary hydroxy group leading to the formation of DHA species. Au is also known to produce C3 deeper oxidized products, such as Tartronate and Mesoxalate, although the latter wasn't observed in the present work [34]. Also, the C2 and C1 deeper oxidized products, such as glycolate, oxalate, formate, and carbonate, corresponding to different oxidized species arising from the GLYOR, were detected [33]. According to literatures [13,34], all these pathways occur on gold-based catalysts.

To further elucidate these reaction steps, all bands were deconvoluted and integrated to determine the contribution of each

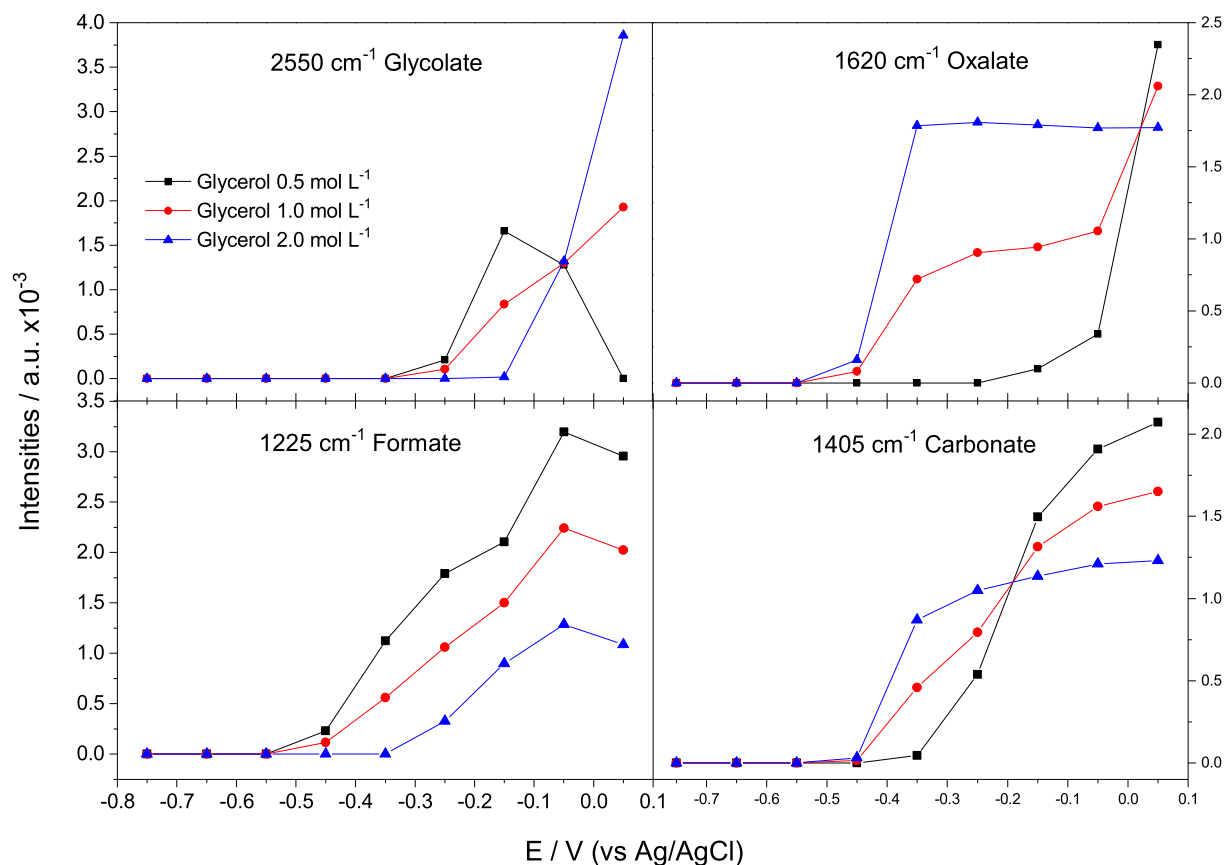


Fig. 8. Glycolate, oxalate, formate, and carbonate integrated intensities bands as a function of the potential. Data extracted from Fig. 4.

product formation depending on the concentration and applied bias voltage. Fig. 5 shows the GLYAD (1071 cm⁻¹) formation as a function of the applied bias voltage. The highest peak for all three concentrations is about ~ -0.55 V and coincides with the shoulder peak in Fig. 3. In the theoretical section, we will explain why the larger intensity is for 0.5 mol L⁻¹ GLY rather than for 1 mol L⁻¹ or 2 mol L⁻¹ GLY.

The disappearance of GLYAD coincides with the start of glycerate, tartronate and C2/C1 species formation, as shown in Figs. 6 and 8. The onset potential for glycerate was almost the same as for tartronate (-0.45 V), which can be explained by the enhanced kinetic reaction: $C_3H_5O_4^- \rightarrow C_3H_2O_5^{2-}$ mediated by the Au surface under the influence of the alkaline medium in Au/C electrocatalyst [35].

Fig. 7 shows the DHA and hydroxypyruvate species formation as a function of the applied bias voltage. The DHA formation can be attributed to either GLY hydroxy group dehydrogenation on C2 or the interconversion with GLYAD. The kinetic reaction for DHA formation is lower compared to that for GLYAD formation, as indicated by the higher onset potential for DHA formation. On the basis of Figs. 5 and 7, for low GLY concentration GLYAD is the main oxidation product, whereas for high GLY concentration DHA is the main oxidation product. As can be seen in Fig. 7, for low GLY concentration a considerable amount of DHA is formed at a higher potential (DHA onset potential -0.15 V) than that for high GLY concentration (DHA onset potential -0.45 V), followed by a fast oxidation to hydroxypyruvate [14,36]. For high GLY concentration, instead, DHA is almost stable.

It is important to stress out again that the mesoxalate is one of

the precursors of the cleavage of the C–C bond, but its IR absorption band could not be identified through our experimental setup. Nonetheless, IR absorption bands related to glycolate, oxalate, formate, and carbonate (Fig. 8) was identified and showed some correlations with the GLY concentration. C2/C1 species can be formed by oxidation of glycerate and tartronate with C–C bond cleavage. For instance, C1 deeper oxidized species production was found to be efficient for lower GLY concentration (0.5 mol L⁻¹), while C2 deeper oxidized species were found to be efficient for higher GLY concentration (2.0 mol L⁻¹) [1,35,36].

Our results corroborate to the idea that a good O–H/C–H scission on the early dehydrogenation process of GLYOR leads to high probabilities of C–C cleavage at deeper stages.

4. Conclusion

In this work the products of GLYOR by an *in situ* ATR-FTIR experiment and by cyclic voltammetry have been investigated, highlighting the effect of GLY concentration on the type of GLY oxidation intermediate species. For low GLY concentrations, the formation of a high amount of glyceraldhyde (GLYAD) was observed, while for high GLY concentrations a lower amount of GLYAD was obtained and the formation of dihydroxyacetone (DHA) was prevalent. For high GLY concentrations, DHA is almost stable, whereas for low GLY concentrations DHA is fast oxidized to hydroxypyruvate. The high GLYOR activity of the Au/C catalyst for low GLY concentrations leads to the formation of deeper oxidized C1 species.

Credit author statement

C.E.D. Ramos: Preparation and execution of electrochemical characterization experiments; preparation of electrocatalysts.

C.A.Ottoni²: Preparation and execution of experiments in Glycerol alkaline.

E. H. Fontes and R.F.B. de Souza: Preparation, execution and discussion of XRD, TEM experiments, Electrochemical experiments and FTIR experiments; Preparation, creation and/or presentation of the published work, specifically writing the initial draft; planning and execution research.

Ermete Antoline: Preparation, creation and presentation of the published work writing the finally draft.

Almir Oliveira Neto: Management and coordination responsibility for the research activity planning and execution; Oversight and leadership responsibility for the research activity planning and execution.

Declaration of competing interest

The authors declare that they have no known competing financial interests or personal relationships that could have appeared to influence the work reported in this paper.

Acknowledgment

We are grateful to CAPES (88882.315566/2019), CNPq (300816/2016-2), and FAPESP (2014/09087-4, 2014/50279-4 and 2017/11937-4) for financial supports.

References

- [1] Y.-B. Choi, N. Nunotani, N. Imanaka, Glycerol production from glycerol over Pt/CeO₂-ZrO₂-Fe₂O₃/SBA-16 catalysts around room temperature in open air system, *Mater. Lett.* 278 (2020), 128392.
- [2] C.A. Martins, M.J. Giz, G.A. Camara, Generation of carbon dioxide from glycerol: evidences of massive production on polycrystalline platinum, *Electrochim. Acta* 56 (2011) 4549–4553.
- [3] J. Schnaidt, M. Heinen, D. Denot, Z. Jusys, R. Jürgen Behm, Electrooxidation of glycerol studied by combined in situ IR spectroscopy and online mass spectrometry under continuous flow conditions, *J. Electroanal. Chem.* 661 (2011) 250–264.
- [4] A.A. Rodriguez, C.T. Williams, J.R. Monnier, Selective liquid-phase oxidation of glycerol over Au–Pd/C bimetallic catalysts prepared by electroless deposition, *Appl. Catal. Gen.* 475 (2014) 161–168.
- [5] B.T.X. Lam, M. Chiku, E. Higuchi, H. Inoue, Preparation of PdAg and PdAu nanoparticle-loaded carbon black catalysts and their electrocatalytic activity for the glycerol oxidation reaction in alkaline medium, *J. Power Sources* 297 (2015) 149–157.
- [6] X. Han, D.J. Chadderton, J. Qi, L. Xin, W. Li, W. Zhou, Numerical analysis of anion-exchange membrane direct glycerol fuel cells under steady state and dynamic operations, *Int. J. Hydrogen Energy* 39 (2014) 19767–19779.
- [7] Z. Zhang, L. Xin, W. Li, Electrocatalytic oxidation of glycerol on Pt/C in anion-exchange membrane fuel cell: cogeneration of electricity and valuable chemicals, *Appl. Catal. B Environ.* 119–120 (2012) 40–48.
- [8] P.-G. Choi, N. Nunotani, N. Imanaka, Efficient production of dihydroxyacetone from glycerol over a Pt/CeO₂-ZrO₂-Bi₂O₃/SBA-16 catalyst, *J. Asian Ceram. Soc.* 6 (2018) 368–373.
- [9] B. Liu, J. Greeley, Decomposition pathways of glycerol via C–H, O–H, and C–C bond scission on Pt(111): a density functional theory study, *J. Phys. Chem. C* 115 (2011) 19702–19709.
- [10] B.N. Zope, D.D. Hibbitts, M. Neurock, R.J. Davis, Reactivity of the gold/water interface during selective oxidation catalysis, *Science* 330 (2010) 74.
- [11] W.C. Ketchie, M. Murayama, R.J. Davis, Promotional effect of hydroxyl on the aqueous phase oxidation of carbon monoxide and glycerol over supported Au catalysts, *Top. Catal.* 44 (2007) 307–317.
- [12] M.A. Sanchez-Castillo, C. Couto, W.B. Kim, J.A. Dumesic, Gold-nanotube membranes for the oxidation of CO at gas–water interfaces, *Angew. Chem. Int. Ed.* 43 (2004) 1140–1142.
- [13] C. Coutanceau, S. Baranton, R.S.B. Kouamé, Selective electrooxidation of glycerol into value-added chemicals: a short overview, *Front. Chem.* 7 (2019).
- [14] J. Nandeha, R.F.B. De Souza, M.H.M.T. Assumpcao, E.V. Spinace, A.O. Neto, Preparation of PdAu/C-Sb₂O₅ center dot SnO₂ electrocatalysts by borohydride reduction process for direct formic acid fuel cell, *Ionics* 19 (2013) 1207–1213.
- [15] A.O. Neto, J. Nandeha, R.F.B. De Souza, G.S. Buzzo, J.C.M. Silva, E.V. Spinacé, M.H.M.T. Assumpção, Anodic oxidation of formic acid on PdAu/C-Sb₂O₅·SnO₂ electrocatalysts prepared by borohydride reduction, *J. Fuel Chem. Technol.* 42 (2014) 851–857.
- [16] E.H. Fontes, R.M. Piasentin, J.M.S. Ayoub, J.C.M. da Silva, M.H.M.T. Assumpção, E.V. Spinacé, A.O. Neto, R.F.B. de Souza, Electrochemical and in situ ATR-FTIR studies of ethanol electro-oxidation in alkaline medium using PtRh/C electrocatalysts, *Mater. Renew. Sustain. Energy* 4 (2015) 3.
- [17] A.O. Neto, M. Brandalise, R.R. Dias, J.M.S. Ayoub, A.C. Silva, J.C. Penteado, M. Linardi, E.V. Spinacé, The performance of Pt nanoparticles supported on Sb₂O₅·SnO₂, on carbon and on physical mixtures of Sb₂O₅·SnO₂ and carbon for ethanol electro-oxidation, *Int. J. Hydrogen Energy* 35 (2010) 9177–9181.
- [18] J.C.M. Silva, L.S. Parreira, R.F.B. De Souza, M.L. Calegari, E.V. Spinacé, A.O. Neto, M.C. Santos, PtSn/C alloyed and non-alloyed materials: differences in the ethanol electro-oxidation reaction pathways, *Appl. Catal. B Environ.* 110 (2011) 141–147.
- [19] C.A. Ottoni, S.G. da Silva, R.F.B. De Souza, A.O. Neto, Glycerol oxidation reaction using PdAu/C electrocatalysts, *Ionics* 22 (2016) 1167–1175.
- [20] J. Qi, L. Xin, D.J. Chadderton, Y. Qiu, Y. Jiang, N. Benipal, C. Liang, W. Li, Electrocatalytic selective oxidation of glycerol to tartronate on Au/C anode catalysts in anion exchange membrane fuel cells with electricity cogeneration, *Appl. Catal. B Environ.* 154–155 (2014) 360–368.
- [21] R.M. Modibedi, T. Masombuka, M.K. Mathe, Carbon supported Pd–Sn and Pd–Ru–Sn nanocatalysts for ethanol electro-oxidation in alkaline medium, *Int. J. Hydrogen Energy* 36 (2011) 4664–4672.
- [22] H. Wang, Z. Liu, S. Ji, K. Wang, T. Zhou, R. Wang, Ethanol oxidation activity and structure of carbon-supported Pt-modified PdSn-SnO₂ influenced by different stabilizers, *Electrochim. Acta* 108 (2013) 833–840.
- [23] M.H.M.T. Assumpção, R.F.B. De Souza, D.C. Rascio, J.C.M. Silva, M.L. Calegari, I. Gaubeur, T.R.L.C. Paixão, P. Hammer, M.R.V. Lanza, M.C. Santos, A comparative study of the electrogeneration of hydrogen peroxide using Vulcan and Printex carbon supports, *Carbon* 49 (2011) 2842–2851.
- [24] M. Mougnot, A. Caillard, M. Simoes, S. Baranton, C. Coutanceau, P. Brault, PdAu/C catalysts prepared by plasma sputtering for the electro-oxidation of glycerol, *Appl. Catal. B Environ.* 107 (2011) 372–379.
- [25] A. Falase, M. Main, K. Garcia, A. Serov, C. Lau, P. Atanassov, Electrooxidation of ethylene glycol and glycerol by platinum-based binary and ternary nano-structured catalysts, *Electrochim. Acta* 66 (2012) 295–301.
- [26] D.Z. Jeffery, G.A. Camara, The formation of carbon dioxide during glycerol electrooxidation in alkaline media: first spectroscopic evidences, *Electrochem. Commun.* 12 (2010) 1129–1132.
- [27] Y. Kwon, S.C.S. Lai, P. Rodriguez, M.T.M. Koper, Electrocatalytic oxidation of alcohols on gold in alkaline media: base or gold catalysis? *J. Am. Chem. Soc.* 133 (2011) 6914–6917.
- [28] C.A. Ottoni, S.G. da Silva, R.F.B. De Souza, A.O. Neto, PtAu electrocatalyst for glycerol oxidation reaction using a ATR-FTIR/single direct alkaline glycerol/air cell in situ study, *Electrocatalysis* 7 (2016) 22–32.
- [29] M. Simões, S. Baranton, C. Coutanceau, Electro-oxidation of glycerol at Pd based nano-catalysts for an application in alkaline fuel cells for chemicals and energy cogeneration, *Appl. Catal. B Environ.* 93 (2010) 354–362.
- [30] J. Cai, H. Ma, J. Zhang, Z. Du, Y. Huang, J. Gao, J. Xu, Catalytic oxidation of glycerol to tartronic acid over Au/HY catalyst under mild conditions, *Chin. J. Catal.* 35 (2014) 1653–1660.
- [31] M. Simões, S. Baranton, C. Coutanceau, Enhancement of catalytic properties for glycerol electrooxidation on Pt and Pd nanoparticles induced by Bi surface modification, *Appl. Catal. B Environ.* 110 (2011) 40–49.
- [32] A.O. Neto, J. Nandeha, M.H.M.T. Assumpção, M. Linardi, E.V. Spinacé, R.F.B. de Souza, In situ spectroscopy studies of ethanol oxidation reaction using a single fuel cell/ATR-FTIR setup, *Int. J. Hydrogen Energy* 38 (2013) 10585–10591.
- [33] N. Worz, A. Brandner, P. Claus, Platinum–Bismuth-Catalyzed oxidation of glycerol: kinetics and the origin of selective deactivation, *J. Phys. Chem. C* 114 (2010) 1164–1172.
- [34] E. Antolini, Glycerol electro-oxidation in alkaline media and alkaline direct glycerol fuel cells, *Catalysts* 9 (2019) 980.
- [35] S.A.N.M. Rahim, C.S. Lee, F. Abnisa, M.K. Aroua, W.A.W. Daud, P. Cognet, Y. Pérès, A review of recent developments on kinetics parameters for glycerol electrochemical conversion – a by-product of biodiesel, *Sci. Total Environ.* 705 (2020) 135137.
- [36] A. Zalinaeva, A. Serov, M. Padilla, U. Martinez, K. Artyushkova, S. Baranton, C. Coutanceau, P. Atanassov, Nano-structured Pd-Sn catalysts for alcohol electro-oxidation in alkaline medium, *Electrochem. Commun.* 57 (2015) 48–51.